This article is published in AIAA Journal and is available for download at following link:
https://doi.org/10.2514/1.J056183

Variable turbulent Prandtl number model for shock/boundary-layer interaction

Subhajit Roy[1], Utkarsh Pathak[2] and Krishnendu Sinha[3]

Indian Institute of Technology Bombay, Mumbai 400076

Interaction of shock waves with turbulent boundary layers can enhance the surface heat flux dramatically. Reynolds-averaged Navier-Stokes simulations based on constant turbulent Prandtl number often give grossly erroneous heat transfer predictions in SBLI flows. This is due to the fact that the underlying Morkovin's hypothesis breaks down in the presence of shock waves; thus, the turbulent Prandtl number can not be assumed to be a constant. In this paper, we develop a new variable turbulent Prandtl number model based on linearized Rankine-Hugoniot conditions applied to shock-turbulence interaction. The turbulent Prandtl number is a function of the shock strength and we propose a shock function to identify the location and strength of shock waves. The shock function also simulates the post-shock relaxation of the turbulent heat flux, akin to that observed in canonical shock-turbulence interaction. The model is combined with the well-validated shock-unsteadiness k-ω model and is applied to the complex shock topology observed in oblique shock-turbulent boundary layer interactions. Comparison with experimental data shows significant improvement in the surface heat transfer rate in the interaction region, both for attached and separated SBLI cases. The shock function is also used to propose a robust form of the existing shock-unsteadiness k-ω model that simplifies the numerical implementation enormously.

[1] Doctoral student, Department of Aerospace Engineering.
[2] Research Assistant, Department of Aerospace Engineering.
[3] Professor, Department of Aerospace Engineering. Senior AIAA Member.

Nomenclature

Pr_T = Turbulent Prandtl number

P_k = Production of turbulent kinetic energy

S_{ij} = Symmetric part of mean strain rate tensor

b'_1 = Shock-unsteadiness damping parameter

M_{1n} = Upstream shock-normal Mach number

r = Density ratio

c_f = Skin friction coefficient

q_w = Wall heat flux

δ_0 = Boundary-layer thickness upstream of interaction

k = Turbulent kinetic energy

ω = Specific dissipation rate of turbulent kinetic energy

μ_T = Turbulent eddy viscosity

κ_T = Turbulent thermal conductivity

$\overline{\rho}$ = Mean density of fluid

ξ_t = Instantaneous shock speed

ψ = Shock function

Subscripts

∞ = Free-stream condition

w = Wall condition

I. Introduction

Shock/boundary-layer interactions (SBLIs) are commonly observed in high-speed flows and they are characterized by a rise in surface pressure and high localized heat transfer. Accurate prediction of surface properties becomes important for high-value aerospace applications. A considerable number of studies have investigated SBLIs occurring in varying conditions and configurations [1]. CFD simulations through Reynolds-averaged Navier-Stokes (RANS) based turbulence models are popular in the aerospace industry. Current turbulence models, however, over-predict the peak heat flux values by considerable margins [2–4], and in this work we systematically study and tackle this problem.

Transport of heat in standard turbulence models is modeled through temperature gradient approximation, with thermal conductivity having molecular and turbulent components. The turbulent part of thermal conductivity is usually written in terms of the turbulent Prandtl number (Pr_T), which is calculated based on Morkovin's hypothesis [5]. A direct mathematical implication of Morkovin's hypothesis is the Strong Reynolds Analogy (SRA). It states that the value of velocity-temperature correlation coefficient is -1, which leads to a theoretical value of $Pr_T = 1$. A value of 0.89 produces results that are in good agreement with the experimental data for turbulent boundary layers. This is not the case for SBLI flows, where the ability of the constant Pr_T approach has been called into question by several authors in the past [6, 7].

A natural progression in the modeling of turbulent heat flux is therefore to vary the Pr_T. Variable Pr_T models have shown improvement in the heat flux predictions in SBLI flows [8–10]. Most of the variable Pr_T models solve two additional transport equations for temperature variance and its dissipation rate. The turbulent Prandtl number is then calculated using the time scale of the temperature variance. The additional partial differential equations have a form similar to the k-ϵ or k-ω equations, and have a large number of source terms. The solution of extra equations thus requires more computational power and invariably increases the cost of computation. Algebraic Pr_T models have been devised to account the Pr_T variation in boundary layers, but they do not consider the effect of shocks [11]. In fact, recent studies of shock-turbulence interaction [12, 13] have revealed interesting and non-intuitive variation of the turbulent heat flux across shock waves. The underlying physical mechanisms should, therefore, be considered for computing the turbulent Prandtl number in SBLI flows.

In this work, a new approach is proposed to vary Pr_T based on the physics of shock-turbulence interaction and subsequently extended to SBLI flows. We derive a relationship between the fluctuating velocity and temperature behind a shock, which is used to develop an expression for Pr_T as a function of shock strength. The proposed variable turbulent Prandtl number model is built upon the previously developed shock-unsteadiness (SU) turbulence model [14]. Compared to conventional models, the shock-unsteadiness correction eliminates the over-amplification of turbulent kinetic energy (TKE) at shock waves. It gives significant improvement in predicting the separation bubble size and the surface pressure distribution in SBLI flows [15]. The computed shock/expansion wave patterns and shock-shock interaction match experimental data closely [16, 17]. Due to its potential, the shock-unsteadiness model has been used widely [18, 19] and is being developed further in recent works [20, 21]. We, therefore, use the shock-unsteadiness k-ω model as the baseline model in this work.

This article is organized as follows. The next section describes the experimental SBLI configuration and test conditions of Schulein [22], which are used to evaluate the proposed variable Pr_T model. A brief review of the governing equations and the shock-unsteadiness modified k-ω model are presented in the following section, along with the numerical method and boundary conditions used in the simulations. Next, we develop the new variable turbulent Prandtl number model based on the shock physics. We also present a novel method to implement the shock-unsteadiness modification developed earlier. This method reduces the total computation time and susceptibility to human error significantly, by incorporating a local variant of the shock-unsteadiness model. The last section presents computed results and these are compared with the experimental data to bring out the efficacy of the variable turbulent Prandtl number model.

II. Test cases

Experiments were conducted by Schulein [22] in the DLR Gottingen Ludwieg tube wind tunnel for oblique shock wave/turbulent boundary layer interaction flows with three different shock deflection angles of 6^o, 10^o and 14^o. All the test cases were performed at Mach 5 for 0.3s in the tunnel. The experimental configuration, shown in figure 1, consists of a flat plate and a shock generator with deflection angle β. The flat plate was kept in the center of test section, while the shock generator was placed axially above the plate. The position of the deflector was varied for each test case to impinge the inviscid shock at a fixed location of 350 mm from the plate leading edge. The incident

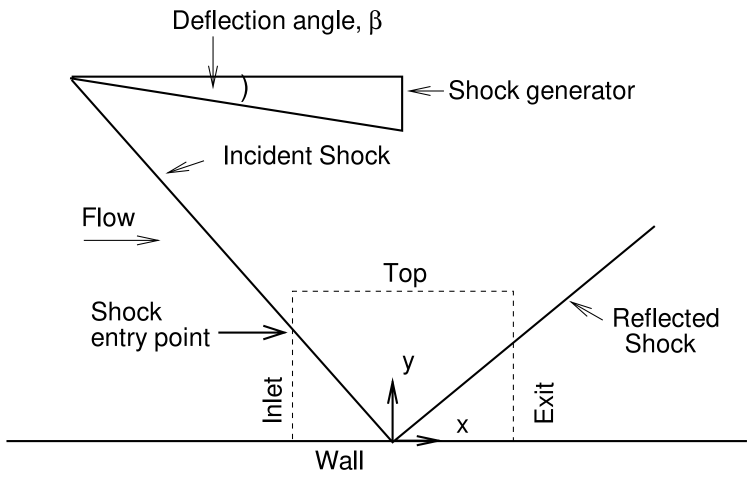

Fig. 1 Experimental configuration of Schulein [22] to study the interaction of an oblique shock with a turbulent boundary layer. Dashed line represents the computational domain, with the boundary conditions marked in the figure.

shock strength increases with higher deflection angle, resulting in a stronger interaction with the turbulent boundary layer developed over the flat plate. The inflow unit Reynolds number, static pressure and temperature are 37×10^6 m^{-1}, 4008.5 N/m^2 and 68.3 K respectively. The flat plate surface temperature is 300 K. Dry air was taken as the test medium with perfect gas assumption. Initially, the experiments were performed for flow over flat plate to develop the undisturbed turbulent boundary layer and the boundary layer properties like δ, δ^*, θ and c_f were measured at different locations. Surface properties like pressure, skin friction and heat transfer rates were obtained along the flat plate in the interaction region.

III. Computational method

In order to compute a compressible turbulent flow using two-equation turbulence model, one needs to solve the Reynolds-averaged Navier-Stokes equations (RANS) for the mean flow along with the transport equations for the turbulence quantities. The standard k-ω model of Wilcox [7] and the shock unsteadiness modified k-ω model of Sinha et al. [15] are used for turbulence closure. The turbulence models do not include any compressibility corrections, as they are found to deteriorate model predictions in the undisturbed boundary layer upstream of the interaction

[23, 24]. Compressibility corrections of the form of dilatational dissipation reduce the turbulent kinetic energy in the boundary layer, and thus decrease the skin friction coefficient compared to well-established correlations for zero pressure-gradient turbulent boundary layers.

A finite volume formulation is used to discretize the governing mean flow equations fully coupled with turbulence model equations. The inviscid fluxes are solved using a modified, low-dissipation form of the Steger-Warming flux splitting method [25]. This method reduces the numerical dissipation, and is found to be useful for high-speed flows with strong shock waves and viscous-inviscid interactions with boundary layers. As a result, very thin and well-defined shock waves are captured over a few grid cells. The discretization method is second-order accurate in space; the details of the formulation can be found in Ref. [26]. The viscous fluxes and the turbulent source terms are calculated using second-order accurate central difference method. The implicit Data-Parallel Line Relaxation (DPLR) method of Wright et al. [27] is used to integrate the equations in time to reach a steady-state solution.

The computational domain is shown in figure 1 by dashed line and it extends to about 14 δ_0 upstream and 25 δ_0 downstream of the shock impingement point. Here $\delta_0 = 5.9$ mm is boundary layer thickness upstream of the shock impingement. No slip and isothermal boundary conditions are used at the wall, while extrapolation condition is applied at the exit boundary of the domain. Inlet profiles are obtained from separate flat plate simulation; the details can be found in Pasha et al. [16]. For the turbulence quantities, the boundary conditions at the wall [28] are prescribed as $k = 0$ and $\omega = 60\nu_w/\beta_1\Delta y_1^2$, where ν_w is kinematic viscosity at the wall, $\beta_1 = 3/40$ and Δy_1 is the normal distance to the grid point nearest to the wall. Following Menter [28], the freestream conditions used for the flat plate simulations are $\omega_\infty = 10U_\infty/L = 8.28 \times 10^3 s^{-1}$ and $k_\infty = 0.01\nu_\infty\omega_\infty = 1.87 \times 10^{-3} m^2/s^2$ where L = 1 m is a characteristic length of the flat plate. For the SBLI simulations, k and ω values at the boundary layer edge in the inlet profile are taken as the freestream conditions at the top boundary.

A. Shock-unsteadiness modification

The accuracy of standard RANS turbulence models, like k-ϵ and k-ω, is limited in high-speed flows involving strong shock waves. This is due to the over-amplification of turbulent kinetic energy across the shock wave by standard models. The over estimation of TKE leads to a more energized boundary layer, which is able to sustain the adverse pressure gradient created by the shock waves for longer, thus delaying flow separation. The over-amplification of TKE is partly due to the fact that the standard models do not consider the unsteady nature of shock wave while interacting with turbulence. Upstream turbulence makes the shock oscillate about a mean position and the amplification of turbulence across an unsteady shock is less compared to its amplification across a steady shock wave. Sinha et al. [14] model the unsteady effect of shock waves in the otherwise steady RANS framework and include the unsteady shock physics into standard turbulence models. The shock-unsteadiness modified turbulence models are found to improve the flow topology significantly, thereby giving better predictions for surface pressure and separation bubble size, in flows with shock-shock and shock-boundary layer interactions [15–17]. In this section, we briefly outline the key features of shock-unsteadiness k-ω model, which is taken as the baseline for implementing the variable Pr_T model.

The production term of the turbulent kinetic energy in the standard k-ω model is given as:

$$P_k = \mu_T \left(2 S_{ij} S_{ji} - \frac{2}{3} S_{ii}^2 \right) - \frac{2}{3} \bar{\rho} k S_{ii} \tag{1}$$

where $S_{ij} = \frac{1}{2} \left(\partial \widetilde{u}_i / \partial x_j + \partial \widetilde{u}_j / \partial x_i \right)$ and $\widetilde{u}_i$ is the component of the Favre-averaged velocity in the i-direction. Here, the overbar and tilde represent the Reynolds and Favre-averaged quantities respectively and the turbulent eddy viscosity is modeled as $\mu_T = \bar{\rho} k / \omega$.

Sinha et al. [14] develop a new transport equation of the TKE with an extra source term to account for the shock-unsteadiness damping effect and it is combined with the production term to get

$$P_k^{'} = -\frac{2}{3} \bar{\rho} k S_{ii} \left(1 - b_1^{'} \right), \tag{2}$$

where μ_T is set to zero in Eq. (1) so as to limit the very high values of $P_k \sim \mu_T (\partial \widetilde{u}_i / \partial x_j)^2$ obtained in shock waves. Here,

$$b_1^{'} = \max.[0, 0.4 \left(1 - e^{1 - M_{1n}} \right)] \tag{3}$$

represents the damping effect of unsteady shock oscillations, and is prescribed using Linear interaction analysis (LIA) results for canonical shock-turbulence interaction. In spite of the limitations of LIA, the shock-unsteadiness model has worked well in SBLI flows [15–17]. The shock-unsteadiness damping parameter is a function of the upstream shock-normal Mach number M_{1n}, which brings in the physical effect of the shock strength. It takes a value of 0.4 in the hypersonic limit and vanishes for very weak shock waves. Additional details of the shock-unsteadiness model development are given in [15].

The shock-unsteadiness modification is applied in the k-ω framework by multiplying the production term of the standard k-ω model by the factor,

$$c_\mu^{'} = 1 - f_s \left[1 + \frac{b_1^{'}\omega}{\sqrt{3}S} \right] \tag{4}$$

where $S = \left[2S_{ij}S_{ji} - \frac{2}{3}S_{ii}^2\right]^{1/2}$ and f_s is an empirical function of the non-dimensional mean dilatation $S_{ii}\delta_0/U_\infty$ [16],

$$f_s = \frac{1}{2} - \frac{1}{2} tanh \left[12 \left(S_{ii}\delta_0/U_\infty\right) + 4\right] \tag{5}$$

It takes a value of one in shocks and high compression regions, such that $c_\mu^{'} = -b_1^{'}\omega/\sqrt{3}S$ and we get the modified production $P_k^{'}$. Otherwise, it is zero and the standard form of k-ω model is recovered outside of shock waves.

IV. Variable turbulent Prandtl number model

The turbulent mode of heat transfer is an important unclosed term in the Reynolds averaged energy equation. In general, the turbulent heat flux vector $q_{T,j}$ is modeled using the gradient diffusion hypothesis

$$q_{T,j} = -\kappa_T \frac{\partial \overline{T}}{\partial x_j}, \tag{6}$$

where κ_T is the turbulent conductivity of heat. It is related to eddy viscosity via the turbulent Prandtl number Pr_T and the specific heat of the gas at constant pressure c_p.

$$\kappa_T = \frac{\mu_T c_p}{Pr_T} \tag{7}$$

Strong Reynolds analogy relates the turbulent heat flux to the Reynolds stress in a boundary layer and thus prescribes a constant value of the turbulent Prandtl number. We use the framework to propose an alternate model for the turbulent heat flux at shock waves in terms of a variable turbulent Prandtl number formulation.

Shock waves enhance turbulence, and lead to a jump in Reynolds stresses, turbulence kinetic energy, vorticity variances and the turbulent dissipation rate. Shock waves also generate large fluctuations in entropy, total temperature and other thermodynamic quantities. The Morkovin's hypothesis [5], based on the assumption of negligible total temperature fluctuations in a flow, therefore breaks down behind a shock wave. Consequently, the velocity temperature correlation coefficient and the equivalent turbulent Prandtl number may vary significantly from their values prescribed by Morkovin's hypothesis. Traditional modeling of the turbulent heat flux in terms of a constant Pr_T thus becomes fundamentally incorrect in regions of shock waves.

Quadros et al. [12] study the turbulent energy transfer when homogeneous isotropic turbulence interacts with a nominally normal shock wave. This is the most fundamental shock-turbulence interaction and it isolates the effects of shock wave on the turbulent transport of heat and momentum. Turbulent energy transfer is quantified in terms of the turbulent energy flux, which is proportional to the turbulent heat flux $q_{T,j}$. It is found that the turbulent energy flux attains a peak value immediately behind the shock, and the post-shock variation is governed by the acoustic decay behind the shock. The location of the peak turbulent energy flux is found to scale with the dissipation length scale that is characteristic of the acoustic disturbances in the flow.

Quadros and Sinha [29] propose improvements to the modeling of turbulent heat flux in canonical shock-turbulence interaction. Scaling relations from Linear Interaction Analysis (LIA) are used to propose a heat-flux limiter model for the turbulent energy flux at a shock wave. The model formulation is similar to the realizable k-ϵ models [30] and matches the DNS values of the peak heat flux for a range of shock strengths. However, being an algebraic model based on the local mean flow properties, it is not able to reproduce the downstream decay in the post-shock flow. Quadros and Sinha [29] also develop a transport equation based model to bring in the history effect of the shock wave in the downstream flow. It includes the downstream decay in terms of the turbulent dissipation length scale and the model predictions match the DNS decay rate up to about one dissipation length behind the shock. This region is expected to be crucial in predicting the wall heat transfer rates, especially in the case of strong SBLI with large separation bubble.

In the current work, we take a simpler approach than [29] and model the turbulent heat flux in terms of a variable turbulent Prandtl number. This is unlike the previous paper, where the turbulent heat flux is modeled directly in the form of an algebraic or differential equation [29]. Being a scalar formulation, the Pr_T approach is easily extendable from one-dimensional canonical shock-turbulence interaction to multi-dimensional SBLI flows. It can also be easily integrated in existing CFD codes, which are traditionally based on constant Prandtl number formulation. In the following, we cast the shock-induced turbulent heat flux into an equivalent turbulent Prandtl number, and propose a variable Pr_T model based on shock-turbulence interaction physics. The variation of Pr_T across a shock wave, if estimated correctly, could improve the heat flux prediction capabilities of the standard turbulence models.

The model is initially developed for a one-dimensional flow through a normal shock, and then extended to two- and three-dimensional flows with oblique and multiple shock waves. The mean flow gradients in the shock-normal direction are very high compared to those in the shock parallel directions. Hence, only the shock-normal component of the velocity and temperature gradients are considered for evaluating the turbulent Prandtl number. The shock-normal Reynolds stress is given in terms of the Boussinesq approximation.

$$-\overline{u'^2} = \frac{4}{3}\nu_T \frac{\partial \overline{u}}{\partial x} - \frac{2}{3}k, \tag{8}$$

where ν_T is the turbulent kinematic viscosity. The first part is proportional to the mean strain rate across a shock and it is much larger than the turbulent kinetic energy contribution to the Reynolds stress. We can thus write

$$\nu_T = -\frac{3}{4}\overline{u'^2}\left(\frac{\partial \overline{u}}{\partial x}\right)^{-1}. \tag{9}$$

Here, the Reynolds averaging procedure is used over Favre averaging, as the difference between the two methods is found to be negligible for Mach numbers upto 6 [12]. Similarly, we can write the thermal eddy diffusivity by applying the gradient-diffusion hypothesis across the shock.

$$\alpha_T = -\overline{u'T'}\left(\frac{\partial \overline{T}}{\partial x}\right)^{-1}, \tag{10}$$

where $\overline{u'T'}$ represents the shock-normal component of the turbulent heat flux vector. The turbulent Prandtl number is thus given by

$$Pr_T = \frac{\nu_T}{\alpha_T} = \frac{3}{4}\frac{\overline{u'^2}}{\overline{u'T'}}\frac{\partial \overline{T}}{\partial x}\left(\frac{\partial \overline{u}}{\partial x}\right)^{-1} \tag{11}$$

The mean flow gradients are computed as part of a RANS solution, and several models are available for the Reynolds stresses, for example, k-ω, k-ϵ, SST, etc. The turbulent heat flux at a shock is estimated as follows.

We consider the conservation of total enthalpy for a turbulent flow passing through a shock wave. It is written in terms of the total temperature in the frame of reference of the shock wave, which undergoes unsteady motion in response to the fluctuations in a turbulent flow. The deviation of the shock from its mean position is taken as $\xi(y,z,t)$, such that the temporal derivative ξ_t represents the instantaneous shock speed in the streamwise direction [31]. The total temperature is written as

$$T_0 = \overline{T} + T' + \frac{(\overline{u} + u' - \xi_t)^2 + v'^2 + w'^2}{2c_p}, \tag{12}$$

by assuming that the shock wave distorts by small angles from its planar mean position. Here, u,v,w are the velocity components, overbar represents mean flow quantity and primes denote turbulent fluctuations. We equate the total temperature between the shock upstream 1 and downstream 2 locations.

$$T_1' + \frac{\overline{u_1}(u_1' - \xi_t)}{c_p} = T_2' + \frac{\overline{u_2}(u_2' - \xi_t)}{c_p}, \tag{13}$$

where the shock speed and the fluctuations are assumed to be small compared to the jumps in the mean flow quantities across the shock. Terms containing squares of fluctuations are therefore neglected. Rearranging the above equation gives

$$T_1' + \frac{\overline{u_1}u_1'}{c_p} = T_2' + \frac{\overline{u_2}u_2'}{c_p} + \frac{\xi_t}{c_p}(\overline{u_1} - \overline{u_2}), \tag{14}$$

where the left hand side represents the linearized form of the total temperature fluctuations upstream of the shock wave. As per Morkovin's hypothesis [5], we can expect the total temperature fluctuations in the upstream flow to be negligible, and this results in

$$T_2' + \frac{\overline{u_2} u_2'}{c_p} = -\frac{\xi_t}{c_p}(\overline{u_1} - \overline{u_2}), \tag{15}$$

which gives an expression for the turbulent heat flux behind the shock wave.

$$c_p \overline{u'T'} = -\overline{u}\left(\overline{u'^2} + \overline{u'\xi_t}(r-1)\right), \tag{16}$$

where r is the mean density ratio across the shock wave and the subscripts are dropped for convenience.

The above expression relates the turbulent heat flux to the streamwise Reynolds stress and can be used to obtain a value of the turbulent Prandtl number. To achieve this, we employ the shock-unsteadiness model of Sinha et al. [14], where the unclosed $\overline{u'\xi_t}$ correlation is written in terms of the shock-normal Reynolds stress component.

$$\overline{u'\xi_t} = b_1 \overline{u'^2}, \quad \text{with} \quad b_1 = 0.4 + 0.6e^{2(1-M_{1n})} \tag{17}$$

This is based on the assumption that the unsteady shock motion is caused by the incoming turbulent velocity fluctuations, and the closure coefficient b_1 is obtained from the linear interaction analysis. The above model for the shock unsteadiness damping correlation accounts for the shock motion at frequencies comparable to that of the incoming turbulence. Additional low-frequency shock oscillations, observed in SBLI, has vanishingly small correlation with the turbulent velocity fluctuations in the boundary layer. Such low frequency shock motion does not contribute to the damping effect in the current framework. We thus get

$$\overline{u'T'} = -\frac{\overline{u}}{c_p}\overline{u'^2}\left(1 + b_1(r-1)\right), \tag{18}$$

which on substitution in Eq. (11) gives the turbulent Prandtl number relation for canonical shock-turbulence interaction.

$$Pr_T = \frac{3}{4}\left(\frac{1}{1 + b_1(r-1)}\right) \tag{19}$$

Here, we have used the mean flow energy conservation to relate the mean temperature and velocity gradients at the shock, assuming minimal contribution from the turbulent kinetic energy to the total enthalpy of the flow.

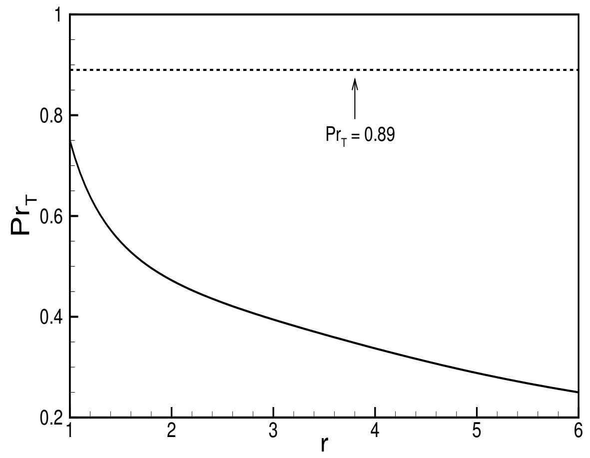

Fig. 2 Turbulent Prandtl number as a function of the density ratio across a shock wave.

Figure 2 shows the variation of Pr_T with shock strength represented in terms of the mean density ratio across the shock. The shock unsteadiness parameter b_1 is also a function of the shock strength, via the shock-normal mean flow Mach number. The turbulent Prandtl number at the shock is lower than the conventionally accepted boundary layer $Pr_{T,0} = 0.89$ and it decreases for stronger shocks. This is consistent with the shock physics, where a stronger interaction has a larger effect on the turbulent transfer of heat and momentum.

DNS data shows that the turbulent energy flux increases dramatically at a shock wave [12]. It attains a peak in magnitude immediately behind the shock and then exponentially decays with distance from the shock wave. In a similar vein, it is reasonable to expect that the turbulent Prandtl number relaxes from its shock value to the conventional value of 0.89 away from the shock, such that the low Pr_T values attained at the shock persists for some finite distance in the downstream flow. Note that a lower Pr_T is equivalent to higher κ_T and higher turbulent heat flux. The post-shock behaviour can be modeled by a differential equation that has an exponentially varying solution behind the shock. The approach is similar to the differential equation model proposed for turbulent energy flux in Ref. [29].

Instead of writing a transport equation for the turbulent Prandtl number, we introduce a scalar shock function ψ and write a transport equation for the same. The objective is that ψ should identify the regions of shock wave in a flow and bring in the history effect of the shock in the downstream flow. The turbulent Prandtl number can then easily be modeled in terms of ψ. The

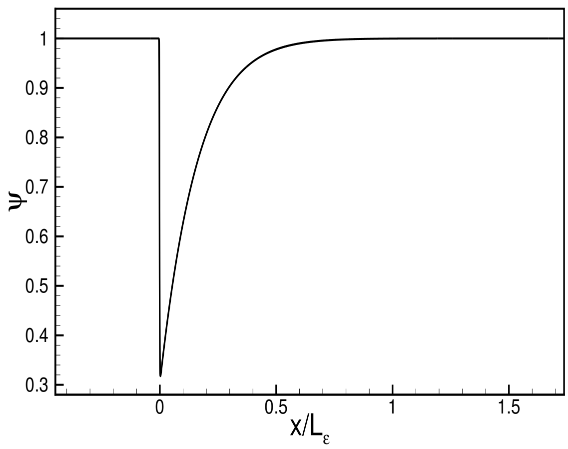

Fig. 3 Streamwise variation of the shock function ψ across a Mach 2.5 normal shock located at x$/L_\epsilon = 0$.

transport equation for ψ is such that it deviates from its undisturbed value ψ_0 only in the regions of strong compression and gradually relaxes back from the shock value to the reference value.

$$\frac{\partial(\bar{\rho}\bar{u}\psi)}{\partial x} = \bar{\rho}\psi\frac{\partial \bar{u}}{\partial x} - \bar{\rho}(\psi - \psi_0)\frac{\bar{u}}{L_\epsilon} \tag{20}$$

Here, the left hand side represents the convection in the shock-normal direction x, the first term on the right-hand side brings in the effect of one-dimensional mean compression, and the second term results in the exponential post-shock variation. Dropping the last term, and integrating across the shock, we get

$$\frac{\psi_s}{\psi_0} = \frac{\overline{u_2}}{\overline{u_1}} = \frac{1}{r}, \tag{21}$$

where the shock value ψ_s is an indicator of the shock strength and an upstream undisturbed value of $\psi_0 = 1$ ensures that we get $\psi_s = 1/r$ at the shock location. Figure 3 shows the variation of ψ in a Mach 2.5 canonical shock-turbulence interaction. The ψ equation is integrated with the shock unsteadiness modified k-ϵ model [20] applied to the one-dimensional mean flow through the normal shock, and the dissipation length $L_\epsilon = \sqrt{k^3}/\epsilon$ is computed using the local values of turbulent kinetic energy and its dissipation rate ϵ. We get a minimum value of $\psi_s = 0.31$ for a density ratio of 3.33 across the shock wave, and it relaxes back to the reference value by $x/L_\epsilon \simeq 1$.

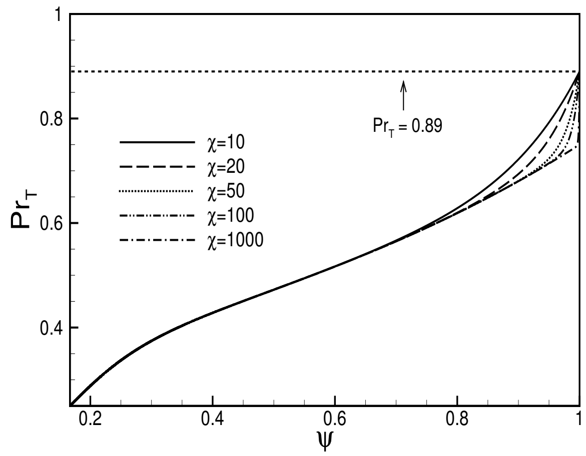

Fig. 4 Effect of the model parameter χ on the variation of the turbulent Prandtl number Pr_T with shock function ψ.

Next, we substitute $r = 1/\psi$ in Eq. (19) to get an expression for turbulent Prandtl number

$$Pr_T = \frac{3}{4}\frac{\zeta}{1 + b_1(\dfrac{1}{\psi} - 1)}, \tag{22}$$

where an additional factor ζ is introduced to make the formulation consistent with the conventionally accepted Pr_T value of 0.89 in boundary layers without shock waves. Thus, ζ is defined as

$$\zeta = 1 + \left(\frac{0.89}{0.75} - 1\right) exp\left(\chi(1 - \frac{1}{\psi})\right) \tag{23}$$

such that it is equal to 0.89/0.75 in the absence of strong compression ($\psi \rightarrow 1$) and approaches 1 in the presence of shock waves. Figure 4 plots the results for ψ ranging from 1/6 (for $M_1 \rightarrow \infty$) to 1 (vanishingly weak shock wave), for a few different values of χ. The parameter χ decides how fast or slow the transition between the shock value of Pr_T and its reference value $Pr_{T,0}$ takes place.

Figure 5 shows the Pr_T computed as a function of streamwise distance for a Mach 2.5 shock wave. It drops from its undisturbed value of 0.89 to about 0.35 at the shock wave, and then exponentially increases back to its reference value. Results are plotted for different values of χ, and it shows the transition from $Pr_{T,shock}$ prescribed by the shock physics to $Pr_{T,0}$. The turbulent Prandtl number approaches the reference level faster for $\chi = 10$, whereas it follows the $Pr_{T,shock}$ values longer for $\chi = 1000$ and switches back to $Pr_{T,0}$ around x $\sim L_\epsilon$. The effect of these differences on the predicted wall heat transfer rate is reported subsequently.

A. Application to canonical shock-turbulence interaction

The current model is applied to the turbulent heat flux generated across a shock wave in canonical shock-turbulence interaction, for which LIA and DNS data is available in Refs. [12, 13, 29, 32]. Quadros et al. [12] study the shock-normal component of the turbulent energy flux $\overline{u'e'}$ in canonical STI. Here, $e = c_v\mathrm{T}$ is the specific internal energy of the fluid, c_v is the specific heat at constant volume and specific enthalpy $h = \gamma e$. We thus have

$$q_{T,x} = \overline{u'h'} = \gamma\overline{u'e'}. \tag{24}$$

In a subsequent work, Quadros and Sinha [29] propose physics-based models for the $\overline{u'e'}$ generated behind the shock wave. The algebraic heat flux limiter model is of particular interest in the current context and will be considered here. The model is developed using results from linear interaction analysis applied to canonical shock-turbulence interaction, and has a form similar to the realizable Reynolds stress models [33]. The model predicts the peak energy flux behind the shock wave and is able to match well with the DNS data of Larsson et al. [32].

We note that the canonical STI cases considered in the previous works [12, 13, 29] have purely vortical turbulence field upstream of the shock. The same is true for the extensive DNS database of Larsson et al. [32, 34], where magnitude of thermodynamic fluctuations are negligible before the shock wave. For such flows, $T_1' = 0$ in Eq. (14) but the contribution of u_1' has to be retained in

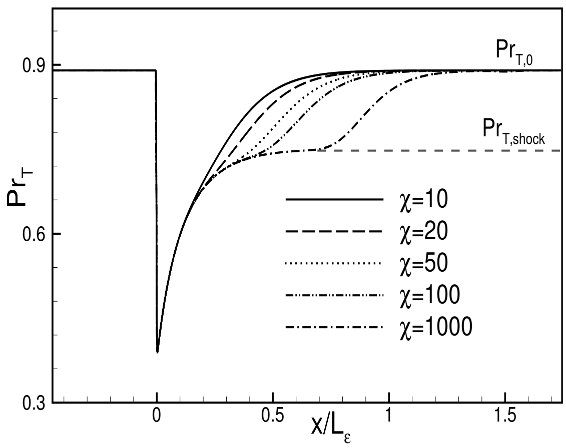

Fig. 5 Variation of turbulent Prandtl number with streamwise distance for a Mach 2.5 shock wave, computed using different values of the model parameter χ.

the derivation. Development similar to that in Eq. (15)-(18) leads to a slightly different form of the turbulent heat flux model for canonical STI.

$$\overline{u'T'} = \frac{\overline{u}}{c_p}\overline{u'^2}\left[(r\alpha - 1) - (r-1)b_1\right], \tag{25}$$

where the additional modeling parameter α relates the upstream and downstream velocity fluctuations; details are provided in appendix A. We adopt the realizable Reynolds stress formulation, similar to Ref. [29], for the shock-normal Reynolds stress, and get the following model for the peak turbulent energy flux correlation in canonical shock-turbulence interaction.

$$\overline{u'e'} = \widetilde{\beta}\frac{k\overline{u}}{\gamma}, \tag{26}$$

where a value of $\widetilde{\beta} = \beta_0 \exp(1 - M_1)$ with $\alpha = 0.6$ matches the DNS data fairly well over the entire range of Mach numbers.

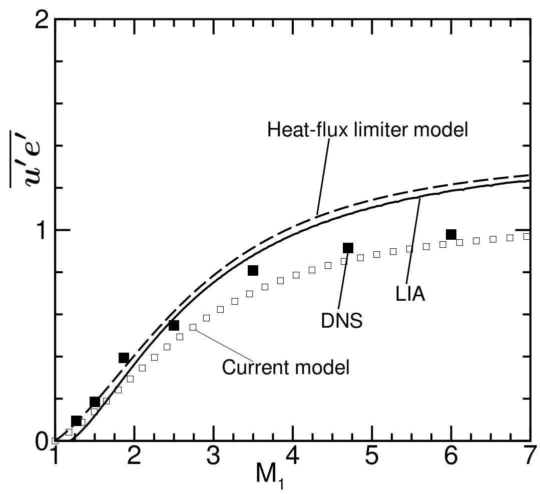

Fig. 6 Peak turbulent energy flux generated in canonical shock-turbulence interaction [12]. The current model is compared with DNS data, LIA predictions and the heat-flux limiter model [29].

B. Extension to shock-boundary layer interaction

For application to real life flows involving multiple shock waves and boundary layer, the transport equation of ψ (Eq. 20) can be written in a general frame-invariant tensor form as,

$$\frac{\partial(\overline{\rho}\psi)}{\partial t} + \frac{\partial(\overline{\rho}\widetilde{u}_i\psi)}{\partial x_i} = \overline{\rho}\psi S_{ii} - \overline{\rho}(\psi - \psi_0)\frac{\sqrt{\widetilde{u}_i\widetilde{u}_i}}{L_\epsilon}, \tag{27}$$

where $\sqrt{\widetilde{u_i}\widetilde{u_i}}$ is the mean velocity magnitude and $L_\epsilon = \sqrt{k}/\omega$ is the dissipation length scale in the k-ω framework. Here, the Reynolds and Favre averaged quantities are used in a way that is consistent with the RANS equations, and the temporal derivative is added for unsteady flows. Further, ψ is artificially kept under the maximum limit of 1 in regions where S_{ii} is positive, such as expansion fans. The transport equation for ψ is solved using the Lax-Friedrich method with explicit time integration. The ψ-solver is decoupled from the main solver for the mean and turbulence model equations described in Section III. A constant CFL of 0.2 is used to update the ψ-function at each time step, and it evolves to attain steady state values in every grid cell, as the flowfield converges to its steady state solution.

The shock function is expected to identify the high compression regions in an SBLI flow. These would include the incident shock, separation shock, reflected shock and others, most of which are oblique in nature. The ψ function computed using Eq. (27) will yield the density jump across the oblique shocks. This corresponds to the strength of the equivalent normal shock. The current model developed for a normal shock wave is thus extended to oblique shocks, as per the local ψ value. This is based on the assumption that the gradients in the shock-normal direction and the corresponding heat flux component plays a dominant role at the shock wave. A more general derivation for oblique shocks will involve transverse velocity fluctuations, and the turbulent Prandtl number will have contributions of the Reynolds shear stresses. The canonical STI problem does not provide information on Reynolds shear stresses, and the current approach will be limited in shock waves that are highly oblique to the incoming flow. An alternate approach would be to extend the current model using Reynolds shear stress data from DNS of SBLI flows. The theoretical framework presented in Ref. [35] to compute post-shock Reynold stresses can be used.

The canonical STI assumes uniform mean flow upstream and downstream of the shock wave. The presence of incoming boundary layer gradients in an SBLI flow can result in a curved shock wave. The shock curvature is governed by the transverse gradient of Mach number, and is expected to be high for hypersonic conditions (see, for example, SBLI flow computations in Ref. [17]). There is a minimal effect of shock curvature in the Mach 5 SBLI cases considered in the current paper; see section V.C for further details.

The linear interaction analysis of canonical STI models a shock wave as a well-defined discontinuity. The linear theory is based on the assumption that the turbulent fluctuations are small compared to the jump in mean properties across the shock. The assumption is compromised in transonic flows (M $\rightarrow$ 1) and near the sonic line in a supersonic or hypersonic boundary layer. It can be physically argued that the effect of the shock is negligible in the limit of Mach number approaching unity, and the turbulence quantities, including the turbulent heat flux, tends to its upstream undisturbed value. This is built into the current model, Eq. (22), where $Pr_T \rightarrow Pr_{T,0}$ when $\psi \rightarrow 1$ for vanishingly weak shock waves.

Further, the LIA framework is based on inviscid flow with a homogeneous isotropic turbulence field upstream of the shock wave. These assumptions are not valid in the near-wall region of a turbulent boundary layer, where low Reynolds number corrections, with damping functions, are often used. In the present context, experimental data suggest that the turbulent Prandtl number is lower than the conventionally accepted value of 0.89 in the log-region of a turbulent boundary layer. A log-layer value of 0.85 is reported for zero pressure gradient boundary layers [11]. Using this value as $Pr_{T,0}$, instead of 0.89, will result in a further reduction of Pr_T across the shock, leading to a lower wall heat flux prediction. This can also be incorporated into the model in the form of a low Reynolds number damping function that will be active in the near-wall region of a turbulent boundary layer.

C. Local formulation of Shock-unsteadiness model

The physics of shock-turbulence interaction is highly dependent on shock strength and the parameter b_1' brings in this effect in terms of the shock normal upstream Mach number M_{1n}; see Eq. (3). This makes the CFD implementation of the shock-unsteadiness model non-local in nature. The flow variables at upstream points of the shock wave are used to evaluate b_1' required to solve the turbulent kinetic energy equation at points in the shock region. Computing M_{1n} is not trivial for flows involving multiple shock interactions [16, 17], where the shock topology is not known a priori. Preliminary simulations are done to get an estimate of the shock location, shape and strength, which are then used to compute b_1' in a subsequent simulation. This increases the computational time and human effort to obtain the final results using shock-unsteadiness model.

In this work, we eliminate the non-local nature of the shock-unsteadiness model. The upstream shock-normal Mach number dependence of the model parameter is replaced by the local density ratio r, which is used to represent the shock strength. The shock-unsteadiness parameter is recast as

$$b_1' = 0.4\left(\frac{r-1}{5}\right)^{0.3} = 0.4\left(\frac{1-\psi}{5\psi}\right)^{0.3}, \tag{28}$$

where the exponent is obtained using least square curve fitting to the original b_1' in Eq. (3), and the local density ratio is written in terms of the shock function ψ. In the undisturbed flow ahead of shock waves, $\psi = \psi_0 = 1$, which implies $b_1' = 0$ and the shock unsteadiness correction is not applied. At shock waves, ψ takes the value $1/r$, as per Eq. (21), and it captures the shock strength for computing the local value of b_1'. Thus the flow-physics of the original shock-unsteadiness model remain unchanged. The exponential decay of ψ in the post-shock flow does not affect the shock-unsteadiness model correction, as $f_s \to 0$ outside of shock waves.

The local shock-unsteadiness model produces similar results to those of the original non-local version of the model [15, 16]. Figure 7 presents the surface properties computed for a 10 degree oblique shock impinging on a turbulent boundary layer. The current results obtained using the local SU k-ω model are almost identical to earlier results of the non-local SU k-ω model [16]. In the

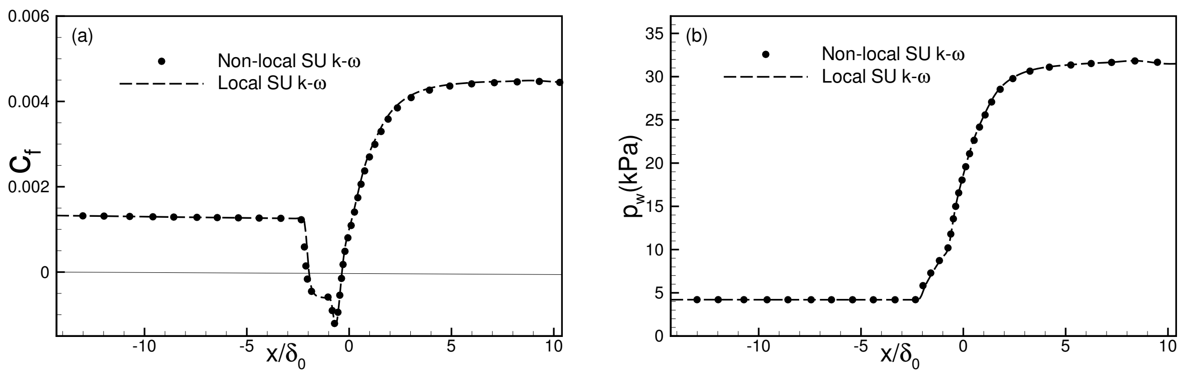

Fig. 7 Comparison of (a) skin friction coefficient and (b) surface pressure for $\beta = 10^o$ oblique shock turbulent boundary layer interaction at $M_\infty = 5$, computed using the non-local SU k-ω [16] and the current local SU k-ω models.

earlier study, the variation of the shock-unsteadiness parameter b_1' was computed manually along the different shock waves in the interaction region, and a mean value of the parameter was used to obtain the final predictions. By comparison, in situ computation of b_1' in terms of the shock-function ψ gives the variation of the model parameter as part of the solution and is directly used in the on-going computation. This results in a 20% reduction in the computational time of the simulation on identical grid. The results obtained for the other cases with 14 and 6 degree shock generators are similar to those presented in Fig. 7 and are not repeated for the sake of brevity.

The model parameter b_1 in Eq. (17) is also recast as

$$b_1 = 0.4 + 0.6 \left(\frac{6 - r}{5} \right)^{5.2} = 0.4 + 0.6 \left(\frac{6\psi - 1}{5\psi} \right)^{5.2}, \tag{29}$$

in terms of local mean density ratio across the shock wave and the shock function ψ. The coefficient 0.4 and 0.6 in the above equation are retained from the original form of b_1 given in Eq. (17). Similarly, the coefficient 0.4 in Eq. (28) is matched to that in Eq. (3). The original form of the model parameters b_1 and b_1' were proposed in Ref. [14] to match LIA data for canonical shock-turbulence interaction. They have been found to work well in SBLI flows over a range of Mach number for different geometric configurations [15–17], and are therefore incorporated into the current model. The exponents in Eqs. (28) and (29) are obtained by curve fitting to the original model coefficients b_1 and b_1' from [14]. A sensitivity study was performed by varying the exponents by up to a factor of 2 and comparing the computed solutions. There is minimal effect on the surface predictions in the current SBLI cases, and the details are omitted for the sake of brevity.

We note that the above formulation is for the SU k-ω model. We can develop local formulation of the shock-unsteadiness corrected k-ϵ and SA models, in a similar way. Also, the variable Pr_T model proposed in this work can be implemented in the k-ϵ framework, using the alternate form of $L_\epsilon = k^{3/2}/\epsilon$. The definition of the dissipation length scale is not trivial for the SA model, and further work is required in this direction.

V. Results

The variable Pr_T model is next applied to oblique shock impingement SBLI flows. Three cases with progressively increasing shock strength are presented, and the predictions of the variable Pr_T

model are compared with those of existing turbulence models. The simulations are performed on 300×400 computational grids, and a detailed grid refinement study is presented in appendix B.

A. 6 degree case

Figure 8 shows the shock structure for an SBLI generated by the 6 degree shock deflector, where the streamwise and wall-normal distances are normalized by δ_0. The solution corresponds to the SU k-ω turbulence model with the variable Pr_T formulation. Figure 8(a) shows that ψ deviates from its reference value of 1 in the regions of shock waves. The same is true for the turbulent Prandtl number; see Fig. 8(b). The regions with $\psi < 0.98$ and $Pr_T < 0.85$ are highlighted in the plots. In the interaction region, ψ is around 0.85 and it results in a Pr_T value of about 0.67. This is about 25% lower than the conventional value of 0.89. Even lower values of Pr_T, in the range of 0.5, are observed in the incident and reflected shocks, but they do not affect the surface heat flux predictions directly.

Figure 9 compares the computed surface properties with the experimental data reported by Schulein [22]. Three turbulence models are used in the simulations, namely, the standard k-ω model, the shock-unsteadiness k-ω and the variable Pr_T formulation added to the shock-unsteadiness k-ω model. All the three turbulence models predict almost identical surface pressure, with a small

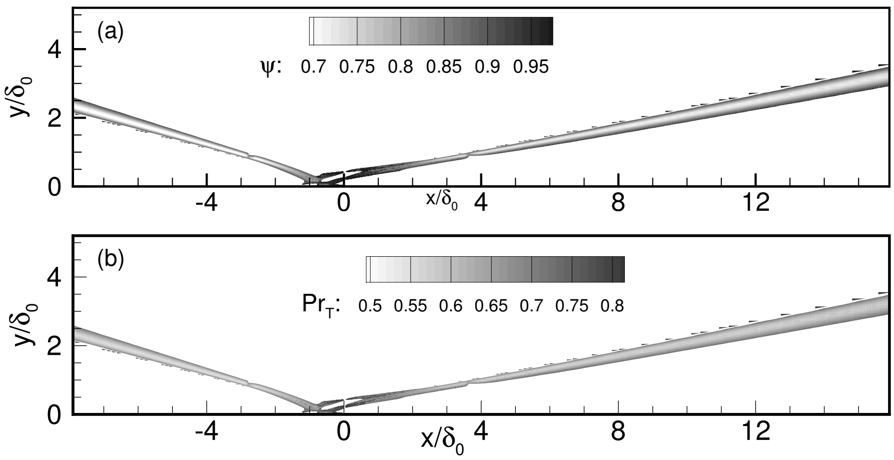

Fig. 8 Distribution of (a) shock function ψ and (b) turbulent Prandtl number for $\beta = 6^o$ and $M_\infty = 5$ shock-boundary layer interaction.

deviation in the vicinity of the shock impingement point. There is a dip in c_f due to incipient separation in k-ω solution, while the shock-unsteadiness model gives a finite, but small separation bubble. This is because of a lower amplification of the turbulent kinetic energy, which enhances flow separation at shock waves. The variable Pr_T form of the SU k-ω model predicts almost identical c_f as that of the constant Pr_T version. Downstream of the interaction region, the SU k-ω results (both constant Pr_T and variable Pr_T versions) are comparable to the experimental c_f measurements; and the results are identical to those presented in Ref. [16].

The heat flux data in Fig. 9(c) shows a trend similar to the skin friction coefficient, with a constant value in the undisturbed boundary layer and a dip in the heat transfer rate at the shock impingement point. The dip is because of the small separation bubble in the SU k-ω solution

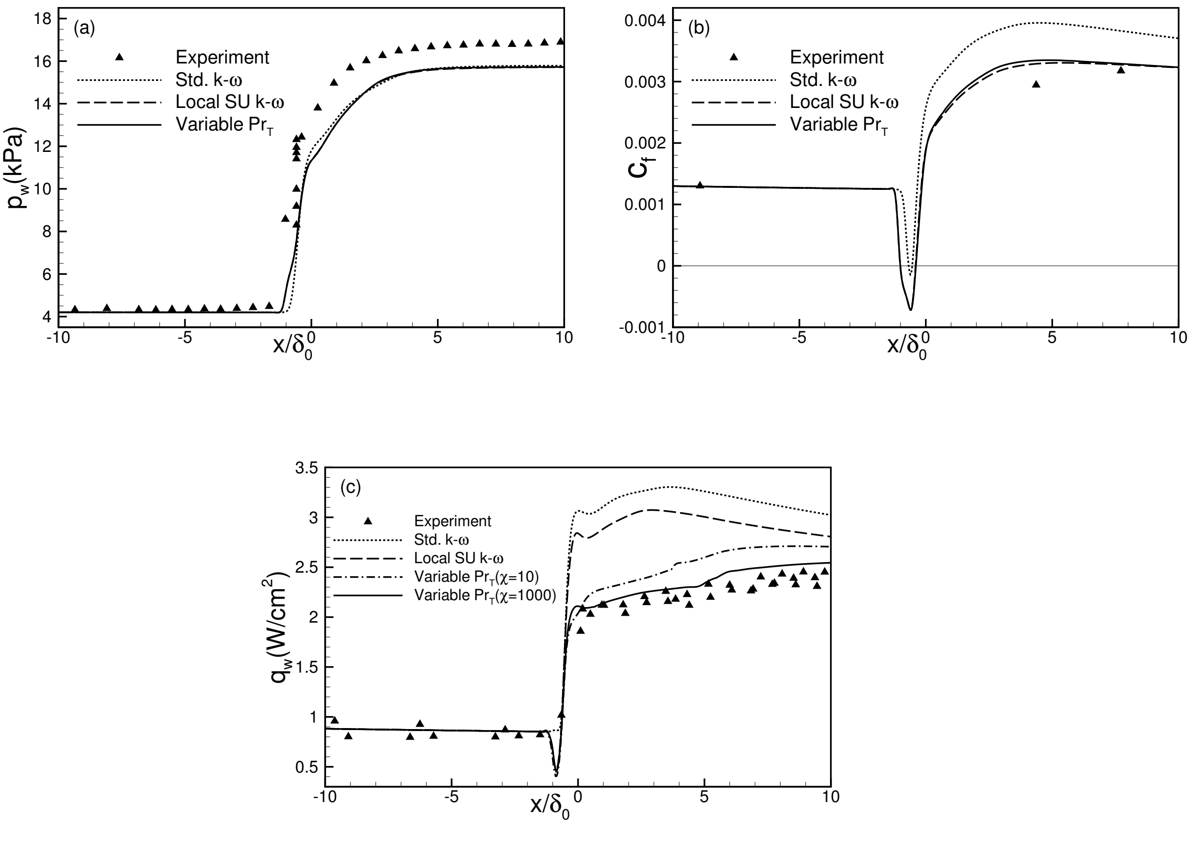

Fig. 9 Comparison of (a) surface pressure, (b) skin friction coefficient and (c) wall heat flux for $\beta = 6^o$ and $M_\infty = 5$ using standard k-ω, shock-unsteadiness modified k-ω and variable Pr_T models with the experimental data of Schulein [36].

and is not seen in case of the standard k-ω model. The experimental data has a sudden jump in surface heat flux, and all three models reciprocate this trend. The standard k-ω model, however, overpredicts the heat flux by about 50%. The shock-unsteadiness correction is found to reduce the surface heat transfer rate, but the results are still substantially higher than the experiment. On the other hand, the variable Pr_T model brings down the post-shock heat transfer dramatically and the results are close to the experiments.

The majority of the data reported in Figs. 8 and 9 correspond to $\chi = 1000$. The only exception is the $\chi = 10$ curve in Fig. 9(c). Using a lower value of χ gives higher surface heat flux, especially in the recovering boundary layer downstream of the interaction region. The heat flux in the vicinity of the reflected shock ($x/\delta_0 \simeq 0$) is relatively unaffected by the change in χ. This is in line with the normal shock data presented in Fig. 5, where all the different values of χ give identical Pr_T near the shock wave. Further downstream, a higher χ retains the low Pr_T values for a longer distance in the downstream flow. For the SBLI configuration, this translates to a lower surface heat flux in the boundary layer recovery region, up to $x/\delta_0 = 10$, as shown in the figure.

Also, note that the standard and shock-unsteadiness k-ω models give a qualitatively different heat flux variation in the recovering boundary layer. There is a peak in the surface heat flux prediction, followed by gradual decrease to levels comparable to the experimental measurements far downstream of the interaction. By comparison, the variable Pr_T model predicts a jump comparable to the measurements, and then a further increase in the recovering boundary layer, akin to what is seen in the experiments.

B. 10 degree case

Experimental data for the 10 degree shock generator shows clear indication of flow separation and the shock-unsteadiness k-ω model reproduces this effect [16]. There are multiple shock waves in the interaction region, with the separation and reattachment points marked as S and R, respectively. Additional details can be found in [16]. The variation of Pr_T, shown in Fig. 10(a) follows the shock pattern closely. There is a region of low Pr_T (in the range of 0.68) in the vicinity of the reattachment point, and it varies along the plate to reach 0.8 at $x \simeq 2\delta_0$.

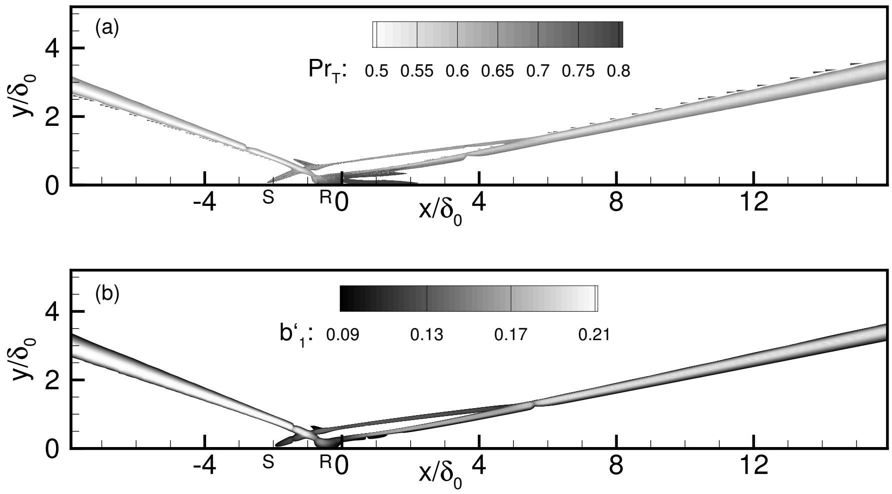

Fig. 10 Distribution of (a) turbulent Prandtl number and (b) shock-unsteadiness parameter b'_1 for $\beta = 10^o$ and $M_\infty = 5$ shock-boundary layer interaction.

The surface heat flux is directly influenced by the variation of Pr_T in the reattachment region and in the recovering boundary layer. Reducing the Pr_T value results in a higher turbulent conductivity as per Eq. (7). An elevated turbulent conductivity leads to a higher diffusion of heat away from the wall, leading to a lower surface heat transfer rate. The model predictions ($\chi = 1000$) match the experimental measurements, both qualitatively and quantitatively, in this region; see Fig. 11. By comparison, the standard and SU k-ω models with constant turbulent Prandtl number predict too high a jump in heat flux at the reattachment point, and they overpredict the data further down-

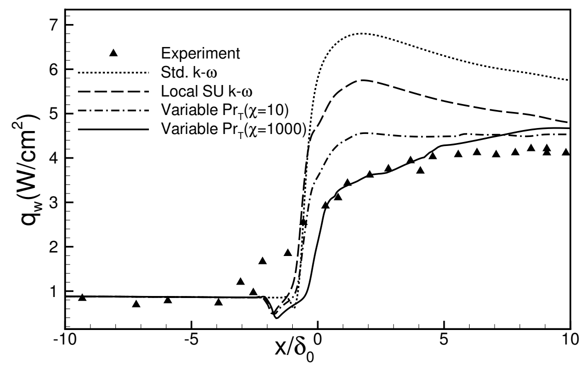

Fig. 11 Comparison of wall heat flux for $\beta = 10^o$ and $M_\infty = 5$ using standard k-ω, shock-unsteadiness modified k-ω and variable Pr_T models with the experimental data [22].

stream. None of the models reproduce the increase in surface heat transfer rate at the separation point, and thus under predict the experimental data in the separation bubble.

The surface heat flux predictions in Fig. 11 show a higher sensitivity to the value of the model parameter χ, as compared to the weaker 6 degree interaction. This is because of the presence of a bigger separation bubble in the 10 degree case that moves the shock waves away from the wall; see the description of shock topology in Fig. 12(a). In such a scenario, the parameter χ plays a crucial role in bringing the effect of the shock waves to the near-wall region. A higher χ results in a lower Pr_T near the surface, and thus a lower surface heat flux is predicted, compared to $\chi = 10$, around $x/\delta_0 = 2$.

The surface pressure and skin friction coefficient are identical to those presented in Fig. 7, as they are not affected by the variation of Pr_T in the interaction region. The SU k-ω model predictions show fair comparison with the measurements, and a detailed comparison with experimental data is presented in [16]. The results are based on the shock-unsteadiness parameter b_1' computed locally in terms of the shock function ψ. The b_1' values are between 0.13 and 0.17 in the interaction region, and increase to 0.21 in the incident shock wave; see Fig. 10(b). The values are indicative of the local shock strength, and b_1' goes to zero outside of shock waves.

C. 14 degree case

The shock pattern computed in the 14 degree SBLI case is similar to the 10 degree case presented before. The incident, induced, transmitted, separation and reattachment shocks are identified in Fig. 12, along with the limiting stream line showing the extent of the separation bubble. A stronger interaction in this case results in large re-circulation region, with about $5\delta_0$ between the separation and reattachment points. Further details of the shock/expansion wave structure can be found in [16].

We note that the separation shock penetrates deep into the boundary layer. A closer inspection reveals that the region identified by the ψ function extends into the log region of the incoming boundary layer. The viscous sub-layer is devoid of shock waves, owing to the low Mach numbers encountered there. The near-wall shock-less region is also characterized by high transverse gradient in Mach number. Relatively smaller variation of the upstream Mach number is found in the region of the separation shock. A lack of substantial curvature of the shock wave (as seen in Fig. 12(a)) corroborates to this fact, and is expected to cause no major limitation to the current model without shock curvature effects. The reattachment and the induced shocks show more pronounced curvature. However, the curved regions are outside the boundary layer and are expected to have minor effect on the surface heat flux predictions.

Experimental data of wall pressure shows a distinct rise at the separation point, followed by a pressure plateau in the separation bubble. The simulation results obtained using the local form of the shock-unsteadiness k-ω model mimic this trend; see Fig. 13(a). The surface pressure past the reattachment point is also predicted well by the model. By comparison, the standard k-ω model gives a separation bubble much smaller than the experiments, and a steeper pressure rise on reattachment. The skin friction data also shows the same behaviour, with the local SU k-ω model predictions matching the experimental measurements well in the separation bubble and reattachment region; see Fig. 13(b). This coincides with the region of peak surface heat flux, and is of direct interest to the present study.

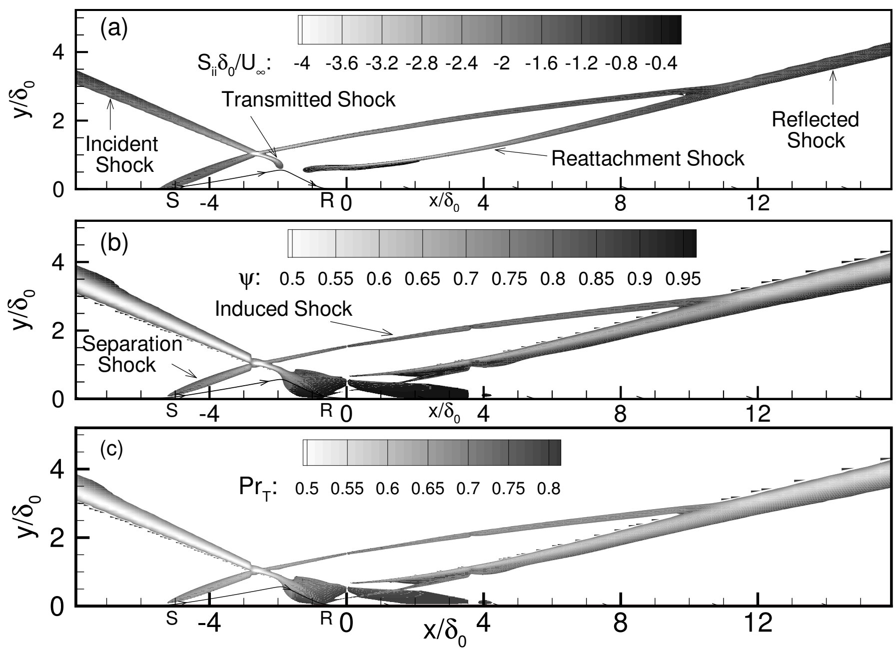

Fig. 12 Distribution of (a) normalized mean dilatation, (b) ψ function and (c) Turbulent Prandtl number for $\beta = 14^o$ and $M_\infty = 5$.

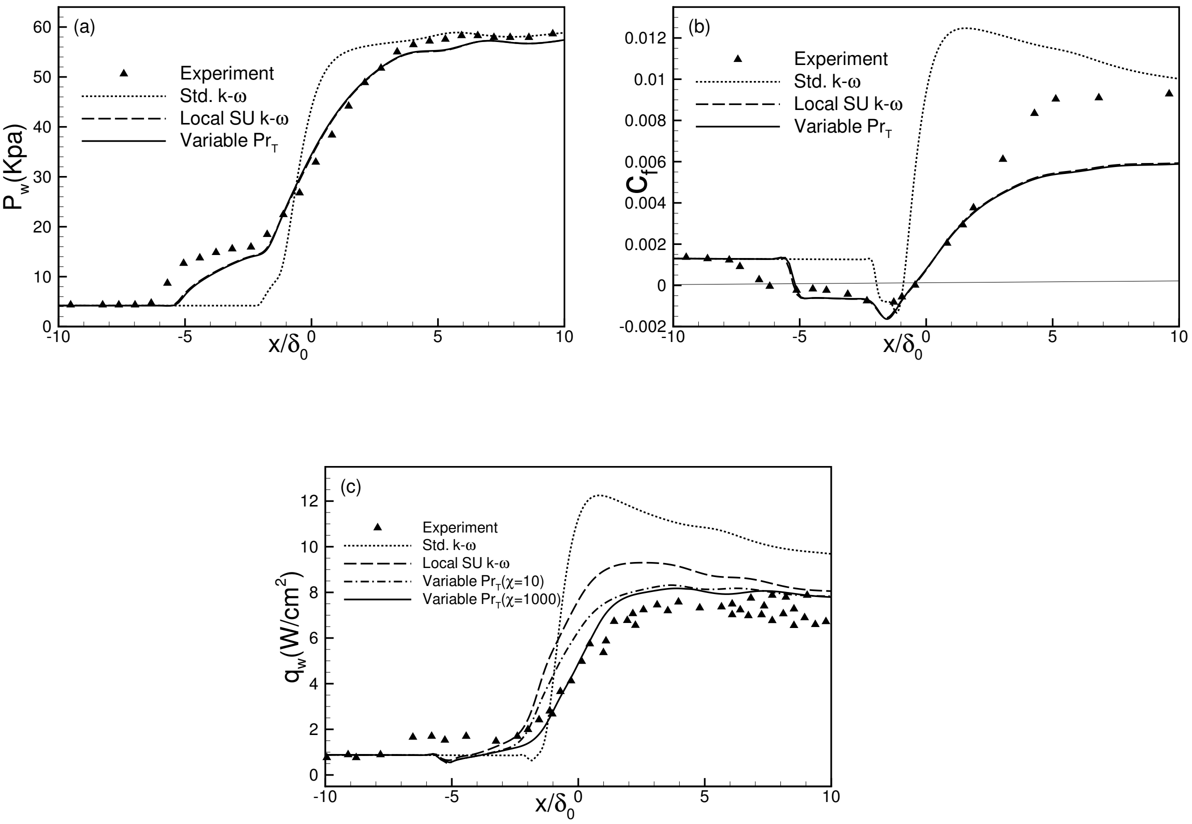

Fig. 13 Comparison of (a) surface pressure, (b) skin friction coefficient and (c) wall heat flux for $\beta = 14^o$ and $M_\infty = 5$ using standard k-ω, shock-unsteadiness modified k-ω and variable Pr_T models with the experimental data [22].

A key feature of the 14 degree SBLI case is that the reattachment shock wave in Fig. 12(a) is oriented parallel to the wall in the peak heat transfer region ($x \simeq 0$). The shock-normal direction is thus oriented towards the wall, such that the turbulent energy transfer in this direction has a direct influence on the surface measurement. Note that the variable Prandtl number model is based on the shock-normal component of the heat flux vector in canonical shock-turbulence interaction. It is therefore expected to capture the heat transfer mechanism directed towards the wall. A similar effect, but to a smaller extent is seen in the 10 degree SBLI case, where the reattachment shock is highly inclined to the wall and a large component of the shock-normal heat flux is in the wall-normal direction.

A second interesting aspect of the 14 degree case is that the reattachment shock is located at the edge of the boundary layer ($y/\delta_0 \sim 0.7$). This is because of the large separation bubble that moves the whole shock structure away from the wall. The reattachment shock or the reflected shock in the weaker interactions penetrates into the boundary layer and it has a direct influence on the heat transfer occurring in the vicinity of the wall. Lowering the turbulent Prandtl number at the shock, therefore, has a large reduction in surface heat flux compared to the SU k-ω prediction. On the other hand, the difference in the peak heat flux predicted by SU k-ω model with constant Pr_T and the current variable Pr_T version is relatively small in the 14 degree case; see Fig. 13(c). Also, varying the parameter χ between its limiting values of 10 and 1000 is found to have minimal effect on the surface heat flux.

The shock waves have an indirect effect on the boundary layer heat transfer via the ψ function, which takes low values in the shock waves and has an exponential relaxation back to its reference value of 1. Thus, the effect of the shock wave is transported in the downstream flow. This can be seen in Fig. 12(b) and 12(c) at the end of the transmitted shock, where low values of ψ and Pr_T are observed in the vicinity of the reattachment point R on the wall. Low values of Pr_T (in the range of 0.8) are also visible along the wall up to x $\simeq 4\ \delta_0$, where the effect of the reattachment shock is carried along the wall by the streamlines passing through the reattachment shock wave. The resulting effect on the surface heat flux can be noted in Fig. 13(c).

Overall, the variable Pr_T model predictions show an excellent comparison with the experimental heat flux measurements in the reattachment region and in the recovering boundary layer. Reducing the eddy viscosity by the shock-unsteadiness correction also gives a reduction in the surface heat flux. By comparison, the standard k-ω model with constant Pr_T overpredicts the peak heat flux by about 70%, and the trends are qualitatively different from that observed in the experiments. This is particularly important in light of the high values of peak heat transfer, up to eight times of the undisturbed boundary layer value, encountered in strong SBLI cases.

VI. Conclusion

In this paper, we use physical insights from canonical shock-turbulence interaction to propose a variable turbulent Prandtl number model for shock-dominated flows. The model is based on linearized Rankine-Hugoniot jump conditions across a shock wave and uses model coefficients derived for the shock-unsteadiness k-ω model developed earlier. As per the analysis, the turbulent Prandtl number takes low values in shock waves, and its value decreases with increasing shock strength. A shock function is used to identify the location and the strength of the shock waves in a flow, and is computed by solving a model transport equation. The model also incorporates an exponential relaxation of the turbulent Prandtl number from its shock value to the conventional value of 0.89 away from shock waves. The shock-unsteadiness model, proposed earlier, is reformulated in terms of the shock function. This removes the upstream dependence of the model parameters, so that they can be evaluated locally at a grid point. The local form of the shock-unsteadiness model is computationally more robust and saves a considerable amount of human effort in a simulation.

The variable Pr_T model is applied, in conjunction with the shock-unsteadiness k-ω turbulence model, to oblique shocks impinging on turbulent boundary layer. Three cases with increasing shock generator angles are computed and the results are compared with the experimental measurements. It is found that the shock function can accurately capture the complex shock topology and the strength of the different shock waves in the interaction region. The low values of the turbulent Prandtl number at the shock waves result in a significant reduction in the surface heat flux prediction. The experimental data is reproduced well, both in terms of the peak heat transfer rate at flow reattachment, as well as the streamwise variation of the surface heat flux in the recovering boundary layer. The computed surface pressure and skin friction coefficient also match the experimental data better than the standard k-ω model. Thus, the current model gives significant improvement for a range of shock-boundary layer interactions, from incipient separation to those involving large re-circulation bubble.

Appendix A. Variable Pr_T model for canonical STI

A variable Pr_T model is developed for canonical shock turbulence interaction where a homogeneous isotropic disturbance field interacts with a normal shock. The initial development is similar to that presented in section IV and it relates the change in total temperature fluctuations across the shock to the unsteady shock oscillation speed ξ_t. We start with Eq. 14

$$T_1' + \frac{\overline{u_1}u_1'}{c_p} = T_2' + \frac{\overline{u_2}u_2'}{c_p} + \frac{\xi_t}{c_p}(\overline{u_1} - \overline{u_2}) \tag{A-1}$$

For purely vortical turbulence upstream of the shock wave, we have $T_1' \to 0$, which leads to

$$T_2' + \frac{\overline{u_2}u_2'}{c_p} = \frac{\overline{u_1}u_1'}{c_p} - \frac{\xi_t}{c_p}(\overline{u_1} - \overline{u_2}) \tag{A-2}$$

Compared to Eq. (15) in section IV, the right-hand side has the additional contribution from the upstream velocity fluctuation u_1'. On taking a moment with u_2', we get

$$\overline{u_2'T_2'} = -\frac{\overline{u_2}}{c_p}\left(\overline{u_2'^2} + \overline{u_2'\xi_t}(r-1) - r\overline{u_1'u_2'}\right) \tag{A-3}$$

The unclosed correlation between the upstream and downstream velocity fluctuations is modeled in terms of the parameter α.

$$\overline{u_1'u_2'} \sim \alpha\overline{u_2'^2}$$

and unsteady shock speed is modeled as per Eq. (17) to get

$$\overline{u'T'} = \frac{\overline{u}}{c_p}\overline{u'^2}\left[(r\alpha - 1) - (r-1)b_1\right], \tag{A-4}$$

where the subscript 2 is dropped for convenience. The above form is identical to Eq. (18) except for α. Substitution into Eq. (11) leads to,

$$Pr_T = \frac{3}{4}\left(\frac{1}{b_1(r-1) - (r\alpha - 1)}\right) \tag{A-5}$$

The turbulent energy flux is modeled in terms of the turbulent heat flux

$$\overline{u'e'} = \frac{\overline{u'h'}}{\gamma} = -\frac{\kappa_T}{\gamma\overline{\rho}}\frac{\partial\overline{T}}{\partial x} = -\frac{\mu_T c_p}{\gamma\overline{\rho}Pr_T}\frac{\partial\overline{T}}{\partial x}, \tag{A-6}$$

where the eddy viscosity μ_T is obtained from a realizable turbulence model [33]. For a normal shock, we have

$$\mu_T = \frac{\sqrt{3c_\mu^o}}{2}\overline{\rho}k\left|\frac{\partial\overline{u}}{\partial x}\right|^{-1} \tag{A-7}$$

which on substitution in Eq. (A-6) yields

$$\overline{u'e'} = \widetilde{\beta}\frac{k\overline{u}}{\gamma}. \tag{A-8}$$

The form is very similar to that proposed by Quadros and Sinha [29], where $\widetilde{\beta}$ is given by

$$\widetilde{\beta} = \beta_0\left(1 - \exp(1 - M_1)\right) \quad \text{ and } \quad \beta_0 = \frac{2}{3}\sqrt{3c_\mu^o}\left[(\mathrm{r}\alpha - 1) - \mathrm{b}_1(\mathrm{r} - 1)\right]. \tag{A-9}$$

Note that the modeling parameter β in the heat flux limiter model [29] is obtained from the hypersonic limiting value of the $\overline{u'e'}$ as per LIA. By comparison, the modeling parameter β_0 is directly derived from the governing equation. It is a function of α which relates the upstream and downstream velocity fluctuations, and is expected to be of order 1.

Appendix B. Grid convergence study

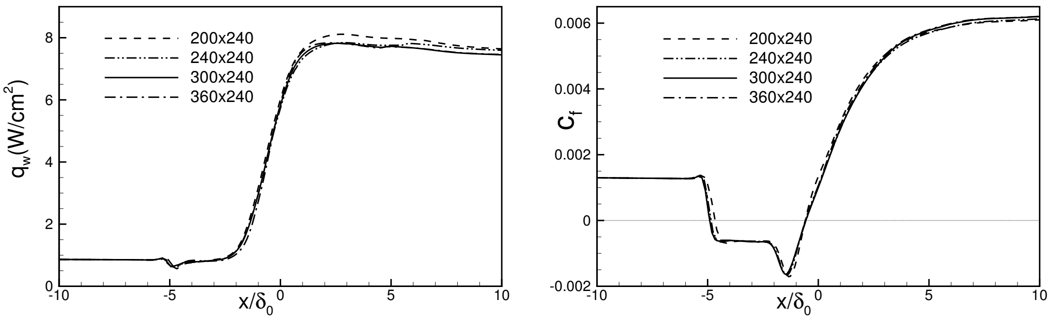

(a) (b)

Fig. 14 Effect of varying number of wall parallel grid points on computed (a) wall heat flux and (b) skin friction coefficient for $\beta = 14^o$ and $M_\infty = 5$.

A structured Cartesian grid is used to capture the strong shock waves, expansion fans and separated flow region. The mesh is stretched exponentially in both wall normal and streamwise directions. The grid points are clustered at $x/\delta_0 = 0$ (point of inviscid shock impingement) and exponential stretching is applied upstream and downstream of the interaction zone. A careful grid refinement study is done by systematically varying the number of grid points in each direction, as well as refining the cell size in the wall-normal direction. The skin friction coefficient is found to be most sensitive to the computational mesh and is used to identify a grid independent solution. Note that the current simulations are done using the local form of the SU k-ω model. A similar grid-refinement study is reported in [16] for the original non-local SU k-ω model applied to identical SBLI cases.

The grid refinement study for the $\beta = 14^o$ strongest interaction is shown here. The variable turbulent Prandtl number model is used to study the grid converged solution. The number of points in the wall parallel direction is refined first. The skin friction and wall heat flux plots in figure 14 indicate that 300 grid points are sufficient for an accurate solution. Next, the number of points in the wall-normal direction is increased until the two finest grid, 300 $\times$ 400 and 300 $\times$ 460, give overlapping solutions in figure 15. Finally, the normal distance of the first cell center from the wall is successively reduced. Figure 16 shows that the first cell center distance of 1×10^{-6} m is sufficient to obtain a grid converged solution. This corresponds to a y_2^+ value of 0.5 or lower in the interaction region. Based on the above grid refinement study, the solution obtained from 300 $\times$ 400 grid points with first cell center distance of 1×10^{-6} m from the wall is considered as grid converged. The same grid is used to generate all the results presented in the paper, including the weaker interaction cases.

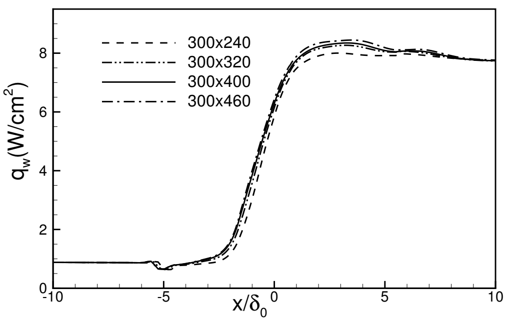

(a)

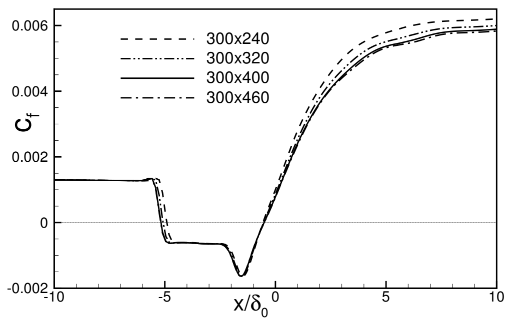

(b)

Fig. 15 Effect of varying number of wall normal grid points on computed (a) wall heat flux and (b) skin friction coefficient for $\beta = 14^o$ and $M_\infty = 5$.

Acknowledgments

The authors would like to thank Indian Space Research Organisation-IITB Space Technology Cell (ISRO-STC) for supporting this research.

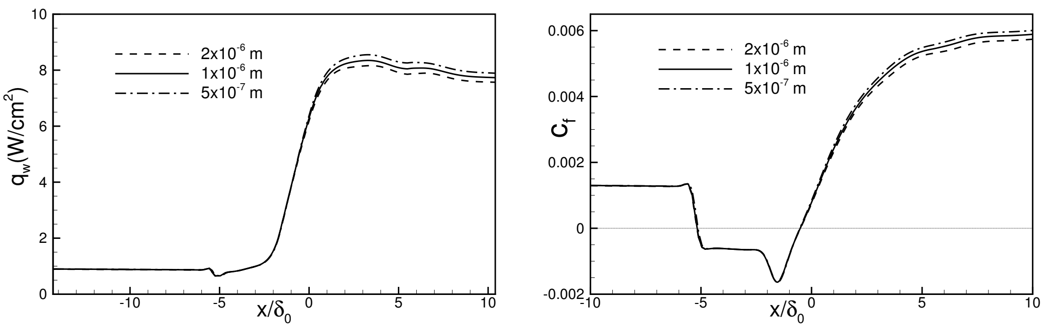

(a) (b)

Fig. 16 Effect of varying wall normal spacing on computed (a) wall heat flux and (b) skin friction coefficient for $\beta = 14^o$ and $M_\infty = 5$.

References

[1] Gaitonde, D. V., "Progress in shock wave/boundary layer interactions," *Progress in Aerospace Sciences*, Vol. 72, 2015, pp. 80-99. doi: 10.1016/j.paerosci.2014.09.002

[2] Brown, J. L., "Hypersonic shock wave impingement on turbulent boundary layers: computational analysis and uncertainty," *Journal of Spacecraft and Rockets*, Vol. 50, No. 1, 2013, pp. 96-123. doi: 10.2514/1.A32259

[3] Roy, C. J., and Blottner, F. G., "Review and Assessment of Turbulence Models for Hypersonic Flows," *Progress in Aerospace Sciences*, Vol. 42, No. 7, 2006, pp. 469-530. doi: 10.1016/j.paerosci.2006.12.002

[4] Leger, J., and Poggie, J., "Computational Analysis of Shock Wave Turbulent Boundary Layer Interaction," 52nd Aerospace Sciences Meeting, Reston, Virginia 13-17 January 2014.

[5] Morkovin, M. V., "Effects of compressibility on turbulent flows," *Mecanique de la Turbulence*, edited by Favre, A., Gordon and Breach, New York, 1964, pp. 367-380.

[6] Bradshaw, P., Launder, B. E., and Lumley, J. L., "Collaborative testing of turbulence models," 29th Aerospace Sciences Meeting, Reno, Nevada 7-10 January 1991.

[7] Wilcox, D. C., "Formulation of the k-ω turbulence model revisited," *AIAA Journal*, Vol. 46, No. 11, 2008, pp. 2823-2838. doi: 10.2514/1.36541

[8] Xiao, X., Edwards J. R., Hassan A. H., and Gaffney R. L., "Role of turbulent Prandtl numbers on heat flux at hypersonic Mach numbers," *AIAA Journal*, Vol. 45, No. 4, 2007, pp. 806-813. doi: 10.2514/1.21447

[9] Ott, J. D., Donald C. K., and Dash, S. M., "Evaluation of Turbulence Modeling Extensions for the Analysis of Hypersonic Shock Wave Boundary Layer Interactions," 51st AIAA Aerospace Sciences

Meeting Including the New Horizons Forum and Aerospace Exposition, Grapevine, Texas 7-10 January 2013.

[10] Dash, S. M., Brinckman, K. W., and Ott, J. D., "Turbulence modeling advances and validation for high speed aeropropulsive flows," *International Journal of Aeroacoustics*, Vol. 11, Nos. 7-8, 2012, pp. 813-850. doi: 10.1260/1475-472X.11.7-8.813

[11] Kays, W. M., "Turbulent Prandtl number - where are we?," *Journal of Heat Transfer*, Vol. 116, No. 2, 1994, pp. 284-295. doi: 10.1115/1.2911398

[12] Quadros, R., Sinha K. and Larsson J., "Turbulent energy flux generated by shock/homogeneous-turbulence interaction," *Journal of Fluid Mechanics*, Vol. 796, 2016, pp. 113-157. doi: 10.1017/jfm.2016.236

[13] Quadros, R., Sinha K., and Larsson J., "Kovasznay Mode Decomposition of Velocity-Temperature Correlation in Canonical Shock-Turbulence Interaction," *Flow, Turbulence and Combustion*, Vol. 97, No. 3, 2016, pp. 787-810. doi: 10.1007/s10494-016-9722-9

[14] Sinha, K., Mahesh K., and Candler, G.V., "Modeling shock unsteadiness in shock/turbulence interaction," *Physics of Fluids*, Vol. 15, No. 8, 2003, pp. 2290-2297. doi: 10.1063/1.1588306

[15] Sinha, K., Mahesh K., and Candler, G.V., "Modeling the effect of shock unsteadiness in shock/turbulent boundary-layer interactions," *AIAA Journal*, Vol. 43, No. 3, 2005, pp. 586-594. doi: 10.2514/1.8611

[16] Pasha, A. A., and Sinha K. "Shock-unsteadiness model applied to oblique shock wave/turbulent boundary-layer interaction," *International Journal of Computational Fluid Dynamics*, Vol. 22, No. 8, 2008, pp. 569-582. doi: 10.1080/10618560802290284

[17] Pasha, A. A., and Sinha, K., "Simulation of hypersonic shock/turbulent boundary-layer interactions using shock-unsteadiness model,“ *Journal of Propulsion and Power*, Vol. 28, No. 1, 2012, pp. 46-60. doi: 10.2514/1.B34191

[18] Zhang, Z., Gao, Z., Jiang, C., and Lee, C.H., "A RANS model correction on unphysical over-prediction of turbulent quantities across shock wave," *International Journal of Heat and Mass Transfer*, Vol. 106, 2017, pp. 1107-1119. doi: 10.1016/j.ijheatmasstransfer.2016.10.087

[19] Emami, B., Bussmann, M., and Tran, H., "Application of realizability and shock unsteadiness to k-ϵ simulations of under-expanded axisymmetric supersonic free jets," *Journal of Fluids Engineering*, Vol. 132, No. 4, 2010, pp. 04-11. doi: 10.1115/1.4001341

[20] Sinha, K., and Balasridhar, S. J., "Conservative Formulation of the k-ϵ Turbulence Model for Shock-Turbulence Interaction," *AIAA Journal*, Vol. 51, No. 8, 2013, pp. 1872-1882. doi: 10.2514/1.J052289

[21] Raje, P., and Sinha, K., "A physically consistent and numerically robust k-ϵ model for com-

puting turbulent flows with shock waves," *Computers & Fluids*, Vol. 136, 2016, pp. 35-47. doi: 10.1016/j.compfluid.2016.05.026

[22] Schulein, E., "Skin friction and heat flux measurements in shock/boundary layer interaction flows," *AIAA Journal*, Vol. 44, No. 8, 2006, pp. 1732-1742. doi: 10.2514/1.15110

[23] Forsythe, J., Hoffmann, K., and Damevin, H.M., "An assessment of several turbulence models for supersonic compression ramp flow," 29th AIAA, *Fluid Dynamics Conference*, Albuquerque, New Mexico 15-18 June 1998.

[24] Coakley, T., and Huang, P., "Turbulence modeling for high speed flows," 30th Aerospace Sciences Meeting and Exhibit, Reno, Nevada 6-9 January 1992.

[25] MacCormack, R. W., and Candler, G. V., "The solution of the Navier-Stokes equations using Gauss-Seidel line relaxation," *Computers & Fluids*, Vol. 17, No. 1, 1989, pp. 135-150. doi: 10.1016/0045-7930(89)90012-1

[26] Sinha, K., and Candler, G. V., "Convergence improvement of two-equation turbulence model calculations," 29th AIAA, *Fluid Dynamics Conference*, Albuquerque, New Mexico 15-18 June 1998.

[27] Wright, M. J., Candler, G. V, and Bose, D., "Data-parallel line relaxation method for the Navier-Stokes equations," *AIAA Journal*, Vol. 36, No. 9, 1998, pp. 1603-1609. doi: 10.2514/2.586

[28] Menter, F. R., "Two-equation eddy-viscosity turbulence models for engineering applications," *AIAA Journal*, Vol. 32, No. 8, 1994, pp. 1598-1605. doi: 10.2514/3.12149

[29] Quadros, R. and Sinha, K., " Modelling of turbulent energy flux in canonical shock-turbulence interaction," *International Journal of Heat and Fluid Flow*, Vol. 61, 2016, pp. 626-635. doi: 10.1016/j.ijheatfluidflow.2016.07.006

[30] Shih, T. H., Liou, W. W., Shabbir, A., Yang, Z., and Zhu, J., "A new k-ϵ eddy viscosity model for high reynolds number turbulent flows," *Computers & Fluids*, Vol. 24, No. 3, 1995, pp. 227-238. doi: 10.1016/0045-7930(94)00032-T

[31] Sinha, K., "Evolution of enstrophy in shock/homogeneous turbulence interaction," *Journal of Fluid Mechanics*, Vol. 707, 2012, pp. 74-110. doi: 10.1017/jfm.2012.265

[32] Larsson, J., Bermejo-Moreno, I., and Lele, S. K., "Reynolds-and Mach-number effects in canonical shock-turbulence interaction," *Journal of Fluid Mechanics*, Vol. 717, 2013, pp. 293-321. doi: 10.1017/jfm.2012.573

[33] Thivet, F., Knight, D. D., Zheltovodov, A. A., and Maksimov, A. I., "Importance of limiting the turbulent stresses to predict 3D shock-wave/boundary-layer interactions," 23rd International Symposium on Shock Waves, Fort Worth, Texas 22-27 July 2001.

[34] Larsson, J., and Lele, S. K., "Direct numerical simulation of canonical shock/turbulence interaction," *Physics of Fluids*, Vol. 21, No. 12, 2009, pp. 1-13. doi: 10.1063/1.3275856

[35] Vemula, J. B., and Sinha, K., "Reynolds stress models applied to canonical shock-turbulence interaction," *Journal of Turbulence*, Vol. 18, No. 7, 2017, pp. 653-687. doi: 10.1080/14685248.2017.1317923

[36] Marvin, J. G., Brown, J. L., and Gnoffo, P. A., "Experimental database with baseline CFD solutions: 2-D and axisymmetric hypersonic shock-wave/turbulent-boundary-layer interactions," NASA Ames Research Center, NASA TM-2013-216604, Moffett Field, CA, 2013.